Available online at www.sciencedirect.com
SCIENCE DIRECT®
Nuclear Instruments and Methods in Physics Research A 499 (2003) 245–263
NUCLEAR INSTRUMENTS & METHODS IN PHYSICS RESEARCH Section A
www.elsevier.com/locate/nima

The RHIC design overview

H. Hahn[a,*], E. Forsyth[a,✠], H. Foelsche[a], M. Harrison[a], J. Kewisch[a], G. Parzen[a], S. Peggs[a], E. Raka[a], A. Ruggiero[a], A. Stevens[a], S. Tepikian[a], P. Thieberger[a], D. Trbojevic[a], J. Wei[a], E. Willen[a], S. Ozaki[a], S.Y. Lee[b]

[a] *Collider-Accelerator Department, Brookhaven National Laboratory, Upton, NY 11973, USA*
[b] *Department of Physics, Indiana University, SW 117, Bloomington, IN 47405, USA*

Abstract

The salient performance objectives for the Relativistic Heavy Ion Collider (RHIC) are presented and the rationale for the design choices of the major collider systems is conveyed. RHIC provides collisions of heavy ions covering the entire mass range from protons to gold. For the prototypical case of Au-on-Au, one obtains energies up to 100 GeV/n per beam and luminosities of $\sim 2 \times 10^{26}\,\mathrm{cm}^{-2}\,\mathrm{s}^{-1}$, averaged over a 10-h storage time. Operation with polarized protons is also possible. The overall accelerator complex used for gold ions consists of the Tandem Van de Graaff, the Booster, the AGS, and the Collider itself, and the scenario for the beam transfer between machines is described. The two separate collider rings cross at six interaction points, where the lattice design provides low-beta insertions for maximum luminosity. The interaction diamond length of <20 cm rms is achieved by bunched beam operation and holding the 56 bunches in a 197 MHz radio-frequency (RF) system after their acceleration in a 28 MHz RF system. The rings are constructed with superconducting magnets, which have a cold bore aperture of 6.9 cm in the arcs. The RHIC specific design challenges posed by intrabeam scattering of heavy ions, passage through transition energy with slow-ramping superconducting magnets, and control of magnetic errors in the low-beta triplet quadrupoles are addressed.

PACS: 01.52.+r; 29.20.−C

Keywords: Heavy; Ion; Collider

1. Introduction

The performance objectives for a generic heavy-ion collider were originally formulated in 1983 by a *Task Force for Heavy Ion Physics* [1]. The finial conceptual collider configuration was subsequently defined in a series of committee meetings and reviews involving the user and accelerator communities as well as the funding agency. While a heavy-ion collider has much in common with the hadron colliders, there are many novel features in a heavy-ion collider that are derived from the special requirements and performance objectives for the heavy-ion experimental program. Furthermore, the availability of an existing empty tunnel, experimental halls, and injector chain at this laboratory, although presenting significant economical advantages, nevertheless imposed certain

*Corresponding author. Tel.: +1-631-344-4246.
E-mail address: hahnh@bnl.gov (H. Hahn).
✠ Deceased in 1995.

0168-9002/03/$ - see front matter
doi:10.1016/S0168-9002(02)01938-1

constraints on the design of the new collider as can be seen in the evolution of the ion collider design at BNL since the initial concepts [2,3]. Salient decisions departing from the previously planned pp machine were the adoption of bunched beam operation, the choice of a single-layer, modest-field, bent superconducting magnet, and the anti-symmetric horizontally arranged lattice [4].

The primary performance capability of RHIC is heavy ion collisions at energies up to 100 GeV/u per beam. With the magnet system set at $B\rho = 839.5\,\mathrm{T\,m}$ for 100 GeV/u Au beams, the operational momentum increases with the charge-to-mass ratio, resulting in kinetic energies of 125 GeV/u for lighter ions and 250 GeV for protons.

The other salient measure of collider performance is the luminosity, which states the number of interactions per unit time per unit cross-section. Luminosities of $2\times10^{26}\,\mathrm{cm^{-2}\,s^{-1}}$ for 100 GeV/u Au-on-Au collisions averaged over the nominal 10 h storage time provides for a productive experimental program. The luminosity values for gold are nominally several orders of magnitude below those of typical pp colliders but due to the large total cross-section for central nuclear collisions, interaction rates are quite comparable. As in the case of hadron colliders, a small diamond length of $<20\,\mathrm{cm}$ rms is desirable for optimum detector design. These high luminosity objectives are best achieved by operation with bunched beams colliding head-on, and it demands a flexible lattice design in which the beta function at the interaction point can be lowered to $\beta^* = 1\,\mathrm{m}$ from the 10 m, the value better suited to injection.

Another design requirement, non-existent in hadron colliders, is to provide collisions between beams of unequal species, most notably protons against Au-ions. Instead of dealing with only one mass and charge state, in heavy ion beams the mass number ranges between 1 and about 200 and the atomic number between 1 and about 80. The parameter of relevance which enters in the design of heavy-ion storage rings is the ratio A/Z which ranges between 1 (for protons) and 2.5 (for Au). The design of a heavy-ion collider must therefore be based on two essentially separate rings capable of operating at different magnetic fields to give the required equal rotation frequencies in the beams. The complexity of the magnet optics required to allow head-on collisions which couples the rings to some degree is most pronounced in the case of protons versus gold and dictates to a large extent the design of the lattice insertion and the immediate interaction point regions. In order to satisfy experimental detector requirements, the insertion region design reserves $\pm8.6\,\mathrm{m}$ free space around each interaction point. The RHIC tunnel and the magnet lattice layout provide for six areas where the circulating beams cross. In principle, this allows for experiments at each interaction point, although one is presently dedicated to accelerator radio-frequency (RF) equipment.

An additional requirement in the design of RHIC is the need of providing collisions between beams of Au-ions over an energy range from top energy down to injection so as to connect to previous experimental results. This requirement is unique, since the typical collider designs primarily emphasize operation at top energy only. RHIC is able to operate over a wide energy range, but the luminosity is energy dependent and is in first approximation proportional to the operating energy. Operation at lower energies has some crucial consequences for the design of the lattice and the choice of the magnet apertures. Heavy ion beams in storage rings require larger aperture magnets because intrabeam scattering due to the Coulomb interaction, which scales with Z^4/A^2, results in increased transverse and longitudinal beam dimensions. The RF requirements of a heavy-ion collider are largely determined by the longitudinal beam dimensions at the end of the storage, which are largest at lower energies. In order to limit magnet aperture, RF voltage, and thus cost, full luminosity and lifetime requirements were specified only for energies above $30\times30\,\mathrm{GeV}/u$.

A collider for heavy ions resembles in many aspects that for hadrons, but the very nature of heavy ions imposes additional constraints and demands on the particle source and the injector facility of the collider. In order to achieve an acceptable luminosity, the collider at injection requires a high number of fully stripped particles, in the case of gold, $\sim1\times10^{9}\ {}^{197}\mathrm{Au}^{79+}$, ions per

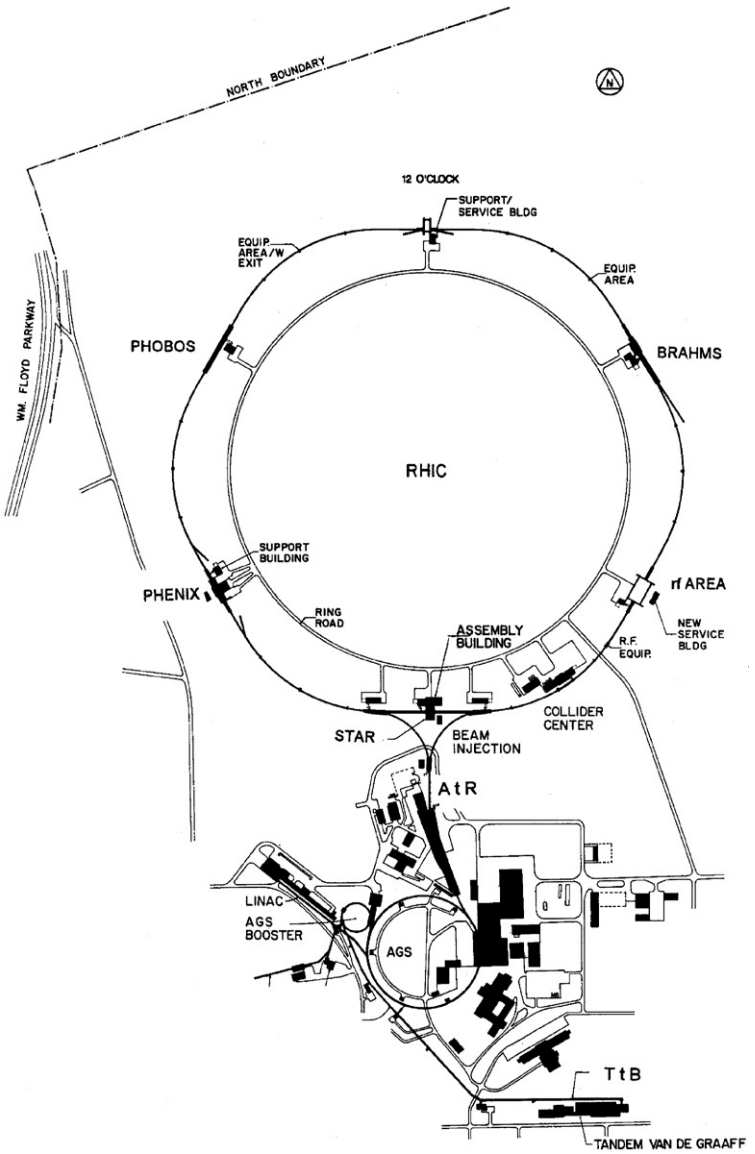

Fig. 1. Layout of the RHIC complex.

bunch contained in a bunch area of $<0.5\,\mathrm{eV\,s}/u$ and in a normalized emittance of $10\pi\,\mathrm{mm\,mrad}$. Operation with the heaviest ions imposes the most demanding requirements on the collider design and operation of gold-on-gold represents the prototypical example. At the other end of the periodic table, proton bunches with $\sim 1\times 10^{11}$ per bunch produce luminosities of $\sim 1\times 10^{31}\,\mathrm{cm^{-2}\,s^{-1}}$. Even though the number of particle differs by two orders of magnitude from gold to proton beams, it is to be noted that the electric current differs by a factor less than two, a fact that simplifies RF and beam observation equipment. Although the existing accelerator facilities at BNL with the injector chain consisting of Tandem van de Graaff pre-accelerator, the Booster Synchrotron, the

Alternating Gradient Synchrotron, and the interconnecting beam transfer lines satisfy the present requirements, studies are in progress addressing future luminosity upgrades by an order of magnitude. Uranium is a viable species but must be considered as a future upgrade, since at the present, an adequate source for uranium does not exist at Brookhaven and further R&D will be needed to achieve this goal. The layout of the RHIC complex with the injector chain and the ring tunnel is shown in Fig. 1.

2. Collider scenario

The scenario describing the operational steps for the overall RHIC accelerator complex can be discussed by aide of Fig. 2. The Tandem Van de Graaff accelerator, after being upgraded to ~ 15 MV, serves for the initial ion acceleration [5]. A two-stage operation is employed with the negative ion source at ground potential. Taking the gold ion as the prototypical example, negative ion beams are extracted from a pulsed sputter ion source (250 μA, <600 μs) [6]. The negative ions, with charge $Q_T = -1$, are accelerated from ground to $+14$ MV potential. They pass through a stripping foil in the high-voltage terminal yielding partially stripped ions, with a positive charge, Q_T, which is a function of the element being accelerated. The partially stripped ions are accelerated back to ground potential, increasing their energy by $14Q_T$ MeV. The gold ions exit the Tandem at the kinetic energy of ~ 1 MeV/u and with $Q_T = +12$ charge state. It is the small emittance and energy spread of the Tandem beams, which permits efficient multi-turn injection into the Booster synchrotron and is a crucial condition to achieve the necessary particle density in the collider [7]. A large variety of ions with adequate intensity can be obtained from the pulsed source providing a remarkable operational flexibility. A second Tandem is available in parallel, which can serve as a spare source of particles or as a source of different ions for an asymmetric collider operation.

Exiting from the Van de Graaff, the gold ions are further stripped to a charge state of $+32$. They then traverse an ~ 850 m long heavy ion transfer line, to the Booster synchrotron without further stripping. The beam from the Tandem is stacked in both horizontal and vertical betatron space by adding linear coupling to the Booster lattice. The 600 μs Tandem pulse yields 45 Booster turns for gold. After multi-turn injection, beams are captured into six bunches and accelerated to 95 MeV/u (431 MeV/c/u). A foil at the Booster exit strips all atomic electrons except for two tightly bound K-shell electrons, so that the 4.3×10^9 ions from the Tandem yield $\sim 2 \times 10^9$ ions from the Booster.

The AGS is filled in four Booster cycles with 24 bunches, debunched and rebunched into four final bunches, and then accelerated, so that each bunch holds ions equivalent to one Booster filling, and which remains bunched throughout the RHIC cycle. The AGS accelerates the gold ions with $Q = +77$ to 8.86 GeV/u (9.75 GeV/c/u) with only a few percent loss. Ions are fully stripped at the exit of the AGS and transported in the AtR beamline to the RHIC storage rings. The design requirements for gold are at this point 1×10^9 ions/bunch in a bunch area of <0.5 eV s/u and with transverse emittances of $\sim 10\pi$ mm mrad. The bunch area containing $\sim 95\%$ of the beam population, S, is defined by $S = 6\pi\sigma_\tau\sigma_E$ where σ_τ is the rms bunch length in units of time and σ_E the rms energy spread. Correspondingly, the normalized emittance, $\varepsilon_N = (\beta\gamma)\varepsilon$, is defined by $\varepsilon = 6\pi\sigma_{H,V}^2/\beta_{H,V}$ where $\sigma_{H,V}$ is the rms beam width or height and $\beta_{H,V}$ the horizontal and vertical amplitude lattice function.

RHIC serves also as a polarized proton collider. The AGS bunches required for the injection into the collider are formed in a different sequence, involving the polarized source, the RFQ, 200 MeV Linac, and Booster. The nominal proton energy in the AGS is 28.3 GeV, although resonances dictate a lower energy for polarized protons, 23.4 GeV (24.3 GeV/c), which determine also the injection energy for heavy ions. The design requirements for protons are 1×10^{10} p/bunch within transverse emittances of $<20\pi$ mm mrad.

The AtR (AGS to RHIC) beam transfer line starts with the fast beam extraction used for the g-2 experiment. The beam line is constructed with

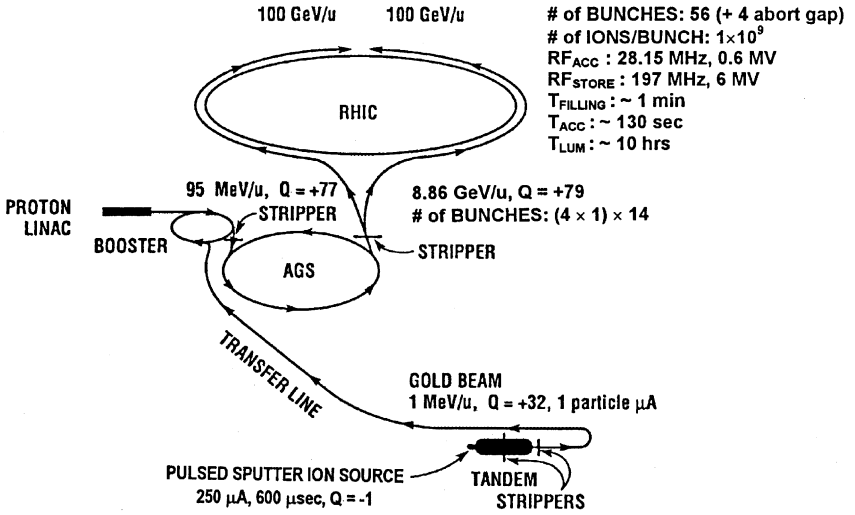

Fig. 2. Acceleration scenario for gold ions.

warm magnets and brings the injected beam into a plane 48 mm above the RHIC median plane. Final injection is performed by a sequence of vertical pitching magnet, horizontally deflecting Lambertson iron septum, and four vertical kicker magnets, each 1.12 m long providing 1.86 mrad at $B\rho = 81.114\,\mathrm{T\,m}$.

Beam injection is done in box-car fashion, one bunch at a time. The AGS cycle is repeated 14 times to establish the 56 bunches in the 360 RF buckets of each ring. Four buckets remain empty for the abort gap. Minimizing the filling time is important in order to prevent bunch area dilution due to intrabeam scattering, with a bunch area of 0.3 eV s doubling in about 7 min. The overall filling time of each ring needs to be done within about 1 min to prevent difficulty in transition crossing. The estimated transverse growth is estimated to be low for the RHIC injection parameters. At the end of the injection cycle, there is a total of $\sim 6 \times 10^{10}$ ions in each ring. For polarized protons and the lightest ions, deuterium, two orders of magnitude more ions are stored in the rings. However, the electrical current, per bunch as well as for the entire ring, is essentially the same for all species, simplifying beam observation and beam control.

The adoption of beam transfer from the AGS to RHIC in the single bunch mode allows considerable freedom in the filling pattern. The minimum number of bunches is six, if collisions at all interaction points are wanted. The nominal case with 60 bunches corresponds to a bunch spacing of 63.9 m. The bunch length of the incoming beam is ~ 20 ns so that the injection kicker rise time must be less than 195 ns. Increasing the number of injected bunches is a possibility only limited by the need to avoid stray collisions and long-range beam–beam effects. The existing kicker has a rise time of ~ 110 ns and allows nominally 72 and 90 bunches per ring. Doubling the number of bunches to 120 will require new units with 95 ns rise times.

The bunches are captured in stationary buckets of the so-called acceleration RF-system operating at 28.15 MHz, corresponding to a harmonic $h = 6 \times 60$. This frequency was chosen to match the bucket shape to the bunch shape determined by the AGS RF system so as to avoid bunch area dilution. The matching voltage of 215 kV is obtained from two accelerating cavities in each ring. Matched transfer at the highest available voltages minimized intrabeam scattering during injection. This RF system performs the capture of the injected beam, its acceleration, and bunch shortening at top energy in preparation for transfer to the storage RF system. To satisfy these functions, the system requires great flexibility with

operating voltages, ranging from 20 to 300 kV/cavity. With the exception of protons, all ion species must be accelerated through the transition energy at $\gamma_T = 22.86$. In order to avoid bunch area dilution at the transition, a fast transition jump must be executed. A rapid change of 0.8 units in 60 ms is achieved by a first-order γ_T jump involving two quadrupole families.

Acceleration from injection to top energy takes about 2 min; faster rates are possible, but the avoidance of eddy current and dynamic magnetization effects simplify operation at this slower rate. After reaching the operating beam energy, in the range from 30 GeV to 100 GeV/u, the bunches are transferred to the so-called storage RF system. The main function of this higher frequency system is to limit the bunch length growth due to intrabeam scattering to <30 cm rms (thereby limiting the collision diamond rms length to <20 cm). This could be achieved with any frequency above ~ 160 MHz, but the availability of phased-out CERN cavities suggested 197 MHz ($h = 7 \times 6 \times 60 = 2520$). The 6 MV required to contain the bunches is provided by seven storage cavities for each beam, with three cavities at 860 kV in each ring, and four cavities in a straight section common to both beams. The bucket length of the storage RF is 1.52 m or 5 ns long. Therefore, in order to transfer the bunch from the acceleration to the storage RF without particle loss, it is of primary importance to start in the AGS with a bunch area of less than 0.5 eV s/u and avoid dilution during the entire acceleration cycle. After acceleration to storage energy, and prior to the transfer, reducing the bunch length is achieved by bunch rotation [8]. The beams in the blue and yellow rings are accelerated together, but need to be synchronized and cogged for collisions only in the storage mode.

At top energy and nominal intensity, the stored beam energy is about 200 kJ per ring for all species. This energy is large enough to cause component damage if lost in an uncontrolled manner but is small enough to be dumped onto an internal beam dump at the end of the storage period or in case of equipment malfunction. The beam will be routinely dumped when the luminosity has declined to an unacceptable level, typically after 10 h, or is aborted whenever deviations from normal operation conditions are detected. The system response time is sufficiently fast to begin safe disposal of the beam within four turns (~ 50 μs) after the dump link signal and is then aborted in a single turn (13 μs) by activating the abort kicker system which deflects the beam onto a dump block. In order to facilitate the abort design, a gap of ~ 1 μs corresponding to four missing bunches will be provided. The beam abort system protects an (un-normalized) $\sim 7\pi$ mm mrad dump aperture, which together with the local beta function defines the minimum aperture of any ring component.

The abort system in each ring is comprised of three major subsystems: (1) the five kicker magnets, (2) the associated pulsers and pulse-forming networks, and (3) the dump absorber [9]. The abort system is located downstream from the 10 o'clock interaction point in a warm section, where beam dynamics favors horizontal deflections. To preserve the integrity of the absorber material, the kicker must disperse the beam bunches over the absorber face, which is achieved by a 50% variation of the deflection strength during the kicker pulse. The most severe requirement occurs with Au beams at top energy immediately after acceleration. In contrast to proton beams, the energy deposition of gold is highest at the dump entrance due to its Z^2 dependence. Since a vacuum window would crack due to thermal shock, the first element of the dump absorber is a stress-resistant carbon–carbon composite placed inside the vacuum chamber. Outside the beam vacuum, the dump consists of graphite, steel and marble blocks.

3. Collider rings

The complete RHIC facility is a complex set of accelerators interconnected by beam transfer lines. The collider part consists of two intersecting superconducting magnet rings in the pre-existing tunnel with four experimental halls, the beam transfer line from the AGS to the collider rings, and the ancillary accelerator systems such as the cryogenic refrigerator system required for the

collider operation. The major parameters for the collider are listed in Table 1.

Bending and focusing of the ion beams is achieved by the ring magnets. In view of the fixed tunnel circumference, a cost optimization indicated that filling the circumference with relatively low-field superconducting magnets is most economical. RHIC operates as an accelerator, as a storage ring, and as a collider for a variety of ion species. It is thus convenient to describe the magnetic performance of the ring magnets by quoting the relevant magnetic rigidity $B\rho$. From this quantity, one can then calculate the beam energy and the other kinematic parameters for all ion species, taking into account the ratio of atomic number over charge, A/Z which in RHIC ranges between 1 (for protons) to ~ 2.5 (for Au). Injection is specified by the common magnetic rigidity value of $B\rho = 81.114\text{l}\,\text{Tm}$. Thus independently of the species being injected, the whole process of acceleration and storage takes the rings from $\sim 81\,\text{T m}$, available from the AGS, to a maximum of 840 T m. An explicit requirement in the design of the ring magnets is the need of providing high-luminosity collisions between beams of Au-ions over an energy range of 30–100 GeV/u. This requirement is unique, since all the other colliders essentially emphasize the design for the operation at top energy only. Operation of RHIC at lower energies had some crucial consequences for the design of the lattice; notably the aperture of the arc magnets was determined to accept the beam growth due to intrabeam scattering at 30 GeV/u.

The nominal design value of $B\rho = 840\text{l}\,\text{Tm}$ is achieved at a magnetic field of about 3.458 T and yields the kinetic energy of 100 GeV/n for Au-ions. Correspondingly, the kinetic energy for protons is 250 GeV. The required field is generated with single-layer cosine-theta magnets, with the dipole current at top energy being 5.1 kA [10]. For maximum operational flexibility, the magnets are contained in vacuum vessels separate for each ring, except those near the collision points. The spacing of the magnets in the arcs is 90 cm between beams.

The collider consists of two rings of superconducting magnets. The main components of the magnet system are 288 arc-size dipoles and 108 insertion dipoles, plus 276 arc and 216 insertion quadrupoles. In addition to dipoles and quadrupoles, there will be an inventory of smaller magnets consisting of 72 trim quadrupoles, 288 sextupoles and 492 corrector magnets at each

Table 1
Major parameters for the collider

Kinetic energy, injection top (each beam),	
Au	8.86–100 GeV/u
Protons	23.4–250 GeV
Luminosity, Au–Au @ 100 GeV/u & 10 h av.	$\sim 2\times 10^{26}\,\text{cm}^{-2}\,\text{s}^{-1}$
No. of bunches/ring	56
No. of Au-ions/bunch	1×10^{9}
Operational lifetime Au @ $\gamma > 30$	~ 10 h
Diamond length	20 cm rms
Circumference, $4\frac{3}{4}C_{\text{AGS}}$	3833.845 m
Beam separation in arcs	90 cm
Number of crossing points	6
Free space at crossing point	± 9 m
Beta @ interaction point, injection, low beta	10 & 1 m
Crossing angle, nominal (maximum)	0 (<1.7) mrad
Betatron tune, horizontal/vertical	28.18/29.19
Transition energy, γ_{T}	22.89
Magnetic rigidity, $B\rho$: @ injection	81.114 T m
@ top energy	839.5 T m
Bending radius, arc dipole	242.781 m
No. of dipoles (192/ring + 12 common)	396
No. of quadrupoles (276 arc + 216 insertion)	492
Dipole field @ 100 GeV/u, Au	3.458 T
Arc dipole length, effective	9.45 m
Arc dipole length, physical	9.728 m
Dipole current	5.093 kA
Arc quadrupole gradient	71 T/m
Arc quadrupole length, effective	1.11 m
Coil i.d. arc magnets	8 cm
Beam tube i.d.	6.9 cm
Operating temperature, helium refrigerant	<4.6 K
Refrigeration capacity at 4 K	24.8 kW
Cooldown time, entire system	~ 7 d
Vacuum, warm beam tube sections	$\sim 7\times 10^{-10}$ mbar
Filling time (each ring)	<1 min
Injection kicker strength, 4 units total (95 ns)	0.186 T m
RF voltage, $h = 360$	600 kV
RF voltage, $h = 2520$	6 MV
Acceleration time ($\text{d}B/\text{d}t = 240$ G/s)	130 s
Beam stored energy	~ 200 kJ
Abort kicker strength, 5 units total	1.34 T m

quadrupole. The arc dipoles have a physical length of 9.728 m (9.45 m effective), are bent with a 4.85 cm sagitta and have a coil aperture of 80 mm in order to accommodate the horizontal "6σ" beam size of ± 27 mm, estimated from intrabeam scattering and magnetic tracking studies. The cold bore beam tube aperture was chosen to be 69 mm in diameter. The beam separation dipole, DX, at the interaction point has a coil aperture of 18 cm, and the dipole in the low beta triplet, where the beam size can be largest, has a coil aperture of 10 cm. The physical aperture of the triplet quadrupoles is 13 cm, a value dictated by available production equipment, but the good field aperture was effectively enlarged by extreme care of the mechanical construction, magnet sorting and the provision of local higher order correctors [11,12].

The magnets are cooled to a temperature of <4.6 K by forced circulation of supercritical helium with a cold circulator [13]. The circulating helium is cooled periodically by liquid helium to supercritical helium heat exchangers called recoolers, which are maintained at operating level by the 25 kW helium refrigerator [14]. The refrigerator also provides 55 kW of refrigeration at 55–70 K to cool heat shields. The primary conductive, current leads, and shield heat loads of the integrated RHIC system were measured to be 8, 4, and 30 kW, respectively. Considering these figures, the refrigerator capacity exceeds the primary heat load by a factor of ~ 2.0 and the secondary by 1.8. The entire cold mass system is 2.15×10^6 kg with a heat content of 1.74×10^{11} J from 4 to 300 K, and can be cooled to steady-state operating conditions in 1 week from room temperature. Upon attaining steady-state operation, temperature variations in the ring magnets are maintained within a tolerance of 0.1 K by the sequence of recoolers around the ring. The refrigerator process cycle is without liquid nitrogen and the electric power requirement of the warm helium compressors is ~ 12 MW nominal and 15 MW maximum. The additional electric power for operating the rings and experiments is 9 MW, and for a full AGS program ~ 10 MW.

The various ring magnets will be excited by an appropriate power supply system, and the magnets are protected by a quench protection system. With the exception of DX, all magnets are self-protecting in case of a quench; however, quench propagation in the ring must be controlled by the protective system.

The beam tube in the superconducting magnets is at the temperature of liquid helium. An extremely good vacuum with a pressure $<10^{-11}$ mbar can be obtained in the absence of leaks into the cold bore. In order to avoid beam loss and radiation background, a vacuum of about 7×10^{-10} mbar is required in the warm beam tube sections of the insertion regions. The cryostats for the superconducting magnets require a separate insulating vacuum of less than 10^{-5} mbar in order to avoid a heat load due to convection.

4. Magnet lattice

RHIC operates as an accelerator, as a storage ring, and as a collider. Each function imposes specific requirements on the lattice of the magnetic elements, which had to be accommodated within the constraints of a pre-existing tunnel. The additional requirements of providing high-luminosity collisions between beams of ions over an energy range from 30 to 100 GeV/u as well as collisions between different ion species, inclusive of polarized protons, has several consequences for the design of the lattice. The lattice adopted has two independent magnet rings in a side-by-side horizontal configuration to accommodate polarized proton operation and is antisymmetric with respect to the six interaction points [15]. The high luminosity performance is achieved by providing tunable low-beta insertions.

The geographical layout of the rings in the RHIC tunnel is shown in Fig. 3. The separation of the two rings is 90 cm between beam axis in the arcs. From a geometric point of view, there is a quasi-sixfold periodicity with six arcs and six straight sections. The small differences between inner and outer arcs give rise to three superperiods. Each superperiod begins with the outer arc, followed by an insertion which takes the beam from the outer to the inner side, the inner arc, and finally the insertion which takes the beam this time from the inner to the outer side. The

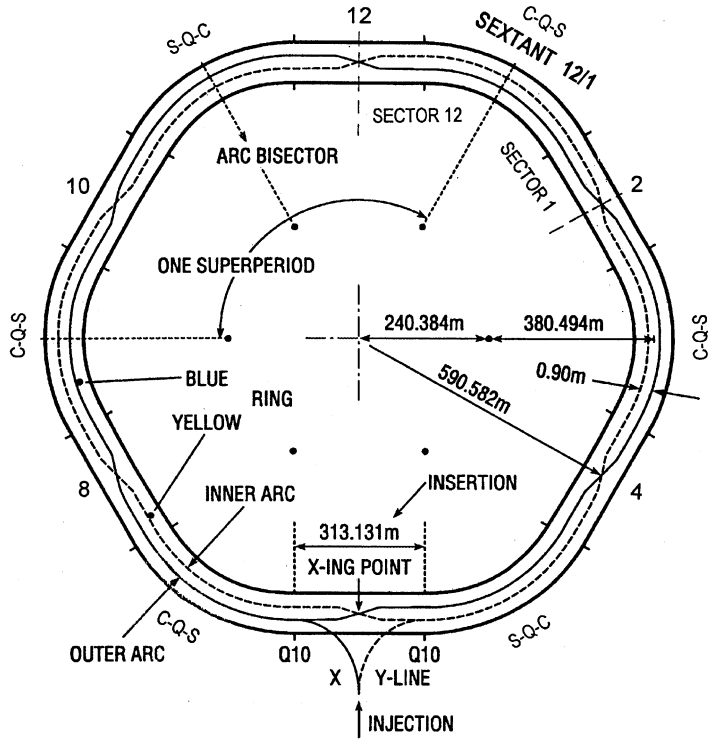

Fig. 3. Ring nomenclature and installation convention.

superperiodicity will be reduced if the insertions are not all identically tuned, e.g. in order to provide different interaction point conditions such as beta values, crossing angles or detector magnets. On the other hand, machine functions, such as beam injection and beam abort, are best accommodated by the standard configuration. It seems advantageous to inject the beam with the highest possible periodicity with all insertions at $\beta^* = 10\,\mathrm{m}$ and depart from this configuration after acceleration in those insertions that require a low β^*.

The two rings are identified as yellow (Y) and blue (B). Beams in the B-ring travel in the clockwise (CW) direction and counter clockwise (CCW) in the Y-ring. The rings cross at six interaction points, which are conveniently identified by their clock positions as 2-, 4-, 6-, 8-, 10-, and 12-o'clock. For the purpose of nomenclature defining the location of a magnet element, the rings are divided into 12 half-sextants, called sectors. Each sector is fully defined by the blue/yellow label, inner/outer position, and clock positions 1–12. The quadrupoles of a sector are numbered consecutively, starting from the crossing point and going either in the CW or CCW direction. The dipoles of a sector are numbered according to their quadrupole position away from the crossing point. The dipole common to both beams near the crossing point is called DX and the dipole ahead of Q1 is consequently D0. Thus, each sector starts with insertion magnets and ends in the arcs at Q21.

The beam in the B-ring follows the convention of the MAD lattice program and serves as reference for the identification in the installation and connections of electrical power supplies. All arc dipoles are installed in CW position, which implies that the beam enters the non-lead end (the lead end) of the dipoles in the blue (yellow) ring. Correspondingly, CW installation of the sextupole–quadrupole–corrector (C–Q–S) assembly unit implies that the blue (yellow) beam enters

the non-lead (lead) end of the quadrupole. The lead end of the corrector is in line with the quadrupole whereas that of the sextupole is opposite. The installation of the arc C–Q–S magnets depends on the sector location and is CW in Sectors 2, 3, 6, 7, 10 and 11 and CCW in 1, 4, 5, 8, 9 and 12. The insertions up to Q9 are geometrically symmetric but electrically antisymmetric with respect to the interaction point. In the triplets, the lead end of Q1 and Q2 is on both sides away from and in Q3 towards the interaction point.

The major magnet parameters for RHIC are presented in the preceding section and a summary is given in Table 1. The circumference of RHIC is 3834 m with an average ring radius of 610 m and the length of one arc being 326 m and that of one insertion 313 m, resulting in an overall packing factor of 40%. The average bending radius in the arcs is 381 m and the dipole-bending ratio is 243 so that the packing factor in the arc cells (that is the ratio of bending radius to average radius) is about 2/3. This low value for the packing factor has detrimental consequences on the lattice performance especially on the chromaticity and the required sextupole strength.

4.1. The arcs

The choice of the arc structure has a profound impact on the performance and cost of the collider. The desire to keep the aperture requirements small points to a lattice solution with stronger focusing and higher transition energy. On the other hand, the requirements of the chromaticity sextupole system, the RF requirements at low energies, and quadrupole cost considerations favor weaker focusing and a lower transition energy.

As a consequence, RHIC is a collider with shorter and stronger focusing FODO cells than those customary in hadron machines. The most important consideration in this regard was the effect of intrabeam scattering. The Au ion bunches experience a significant emittance growth in both transverse and longitudinal planes due to this phenomenon. The long-term diffusion rate, after the equilibrium between longitudinal and transverse dimensions has been reached, is minimized by an arc lattice design in which there are many cells and which has a large phase shift per cell (even beyond 90°), implying both short and strongly focusing cells. An upper limit on the focusing strength was established by the desire to keep the transition below the proton injection energy and the phase shift at or below 90°, to avoid extreme sensitivity to lattice errors. This is achieved in an economical way by adopting an RHIC half-cell with one dipole and one quadrupole.

Each sextant arc is built up with 11 regular FODO cells. The layout of a cell is displayed in Fig. 4 with the cell betatron and dispersion functions. Each cell is ~ 29.622 m long; and it deflects the beam by 77.85 mrad. Its betatron phase advance varies from $\psi_H = 80.55^\circ$ and $\psi_V = 85.40^o$ to $\psi_H = 82.42^o$ and $\psi_V = 87.25^o$ when changing from $\beta^* = 10$ to 1 m, respectively. The maximum lattice function values, in the middle of the regular quadrupoles QF and QD, are $\beta = 49.2$ m and $\eta = 1.74$ m. It is worth noting that there is a single dipole magnet per half-cell, and sextupoles and correction magnets are located next to each quadrupole in the arcs. Lumped correctors are adequate in the absence of strong persistent current fields in the dipoles. Because of the short length of the cells and the presence of inner and outer arcs, it was found convenient to place the dipole magnets exactly half-way between the quadrupoles.

Several hours of storage conditions are expected to result in physically large beams with large energy spreads. Intrabeam scattering calculations indicate for 30 GeV/u gold beams after 10 h, a normalized transverse emittance of 34π mm mrad and $\pm 5 \times 10^{-3}$ momentum spread. This leads to aperture requirements of 18 mm "6σ" betatron amplitude plus 9 mm momentum aperture. Applying the simplistic "2/3" rule together with budgetary considerations leads to the 8 cm coil i.d. which was adopted for all arc magnets. The cold-bore vacuum chamber is a circular pipe of the same cross-section throughout all the arcs, with the internal diameter of 69 mm. Ensuring that the dynamic aperture of the machine is sufficient to result in acceptable luminosity lifetime under these extreme conditions was the main

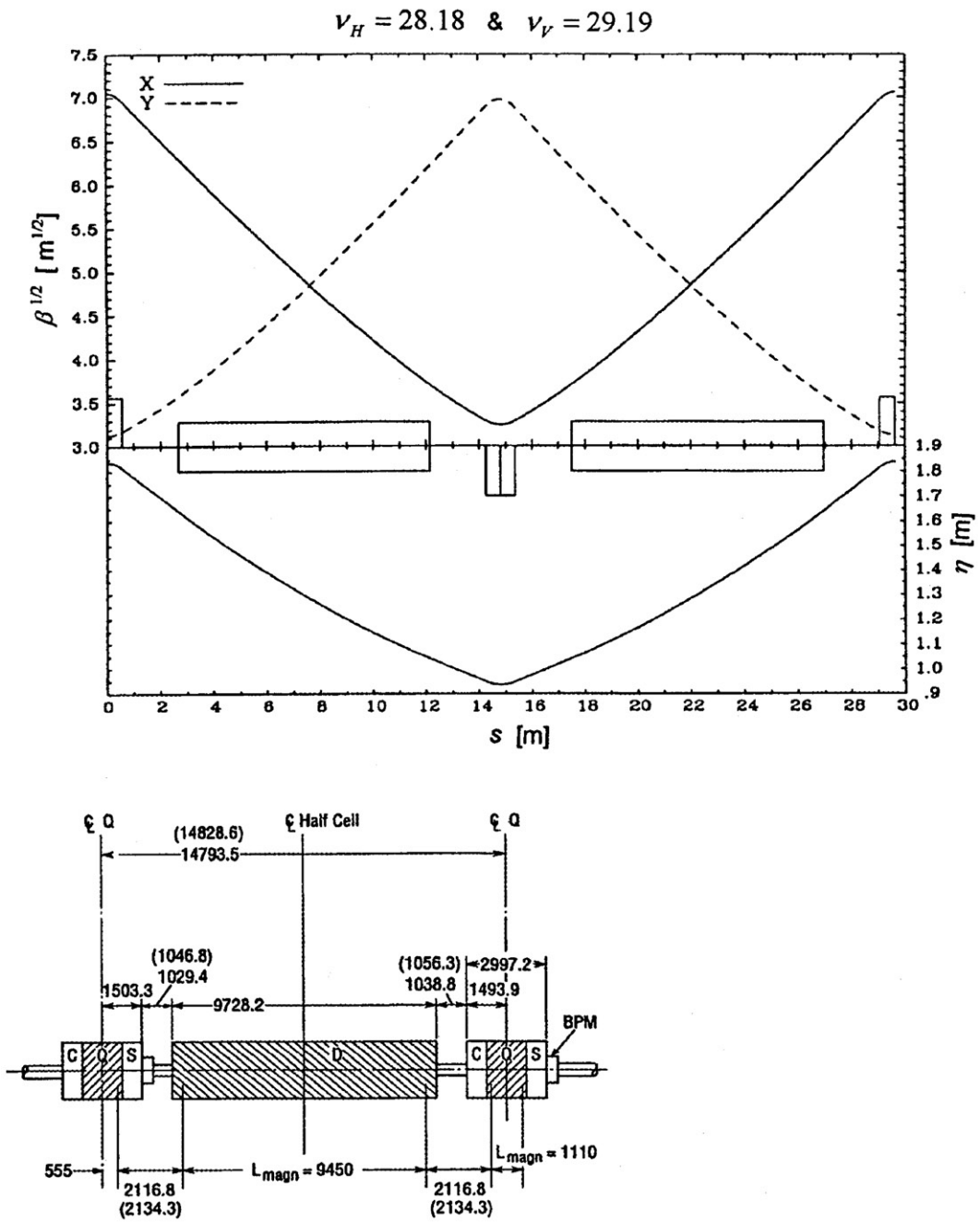

Fig. 4. Layout of inner (outer) arc half-cell, and β and η lattice functions.

factor in adopting the arc magnet and cell parameters. Long-term tracking studies predicted and now the running experience have confirmed that the arc regions allow sufficient aperture and beam lifetime for both the injection process and storage.

4.2. The insertions with the interaction region

The beams cross at the interaction point (IP) of the insertion regions, and their design determines the key parameters for the collider performance. The insertions contain the optics necessary for producing a small betatron amplitude function, β^*, and zero dispersion at the interaction point, plus the bending magnets to bring the beams together [16]. The insertions provide the additional functions for beam injection and beam dump.

One notable approach taken in the conceptual RHIC design is the absence of distinction between utility insertions and experimental insertions. In RHIC, all insertions have the same design, though they may be tuned to somewhat different β^* values. This has the advantage of allowing up to six fully developed experimental areas. In fact, the 6 o'clock insertion co-hosts the large STAR experiment and in 10 o'clock PHOBOS coexists with the beam abort system. Only 4 o'clock remains dedicated to the RF system with common storage cavities in the common beam line, and a wall current monitor at the crossing point.

Fig. 5 shows the sequence of magnets in one half of a long straight section, demonstrating the merging of the two beams at the collision point. Typical behavior of the lattice functions, amplitude and dispersion, are plotted in Fig. 6 for $\beta^* = 1$ m. At the interaction point between two DX magnets is a 17.2 m long, warm magnet-free straight section for experimental detectors. The beryllium beam tube in the detector region is 14.28 m long. Each insertion begins and ends at an inner or outer Q10 but has opposite focusing properties. Thus each insertion starts with a QF and ends with a QD quadrupole and vice versa. The arcs, accordingly, alternate from outer QF10-to-QF10 to inner QD10-to-QD10 configuration.

Like all present-day hadron colliders, RHIC makes use of bunched beams with the same horizontal and vertical transverse emittances. The optimum luminosity performance is then reached with head-on collision and the same focusing properties at the interaction point in both the horizontal and vertical direction. To achieve this, an antisymmetric insertion was adopted, rather than a symmetric one, since it results in equal phase advance in both planes and introduces less chromatic effects. The preferred solution would be to focus both beams to the same spot size with common quadrupoles. This method is very effective in obtaining very low β^*-values since the innermost quadrupoles can be placed close to the interaction point. This standard technique of using common quadrupoles cannot be used at RHIC when the two beams in collision are particles of different species and therefore require different magnetic rigidity. Thus the design of the RHIC interaction region is inverted, with the final focusing quadrupoles being separate for each ring and placed beyond the common DX dipoles that split the two beams. This results in a large distance between the triplet quadrupoles, and in turn limits the lowest beta achievable at the interaction point. A further consequence of operation with unequal species is the need for an enlarged aperture of 18 cm in the common DX magnet.

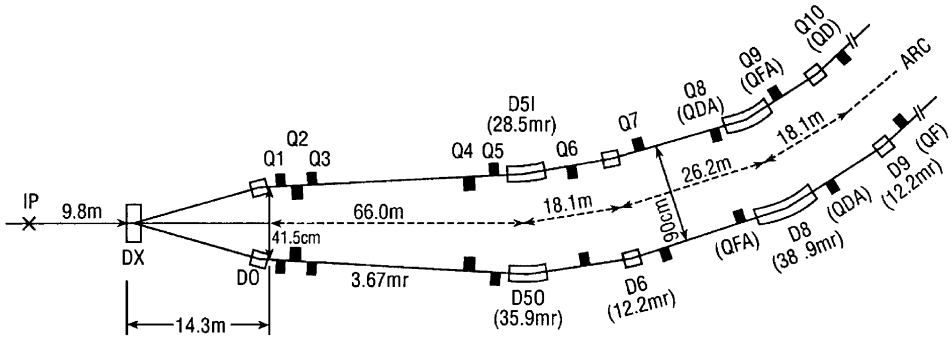

Fig. 5. Insertion layout.

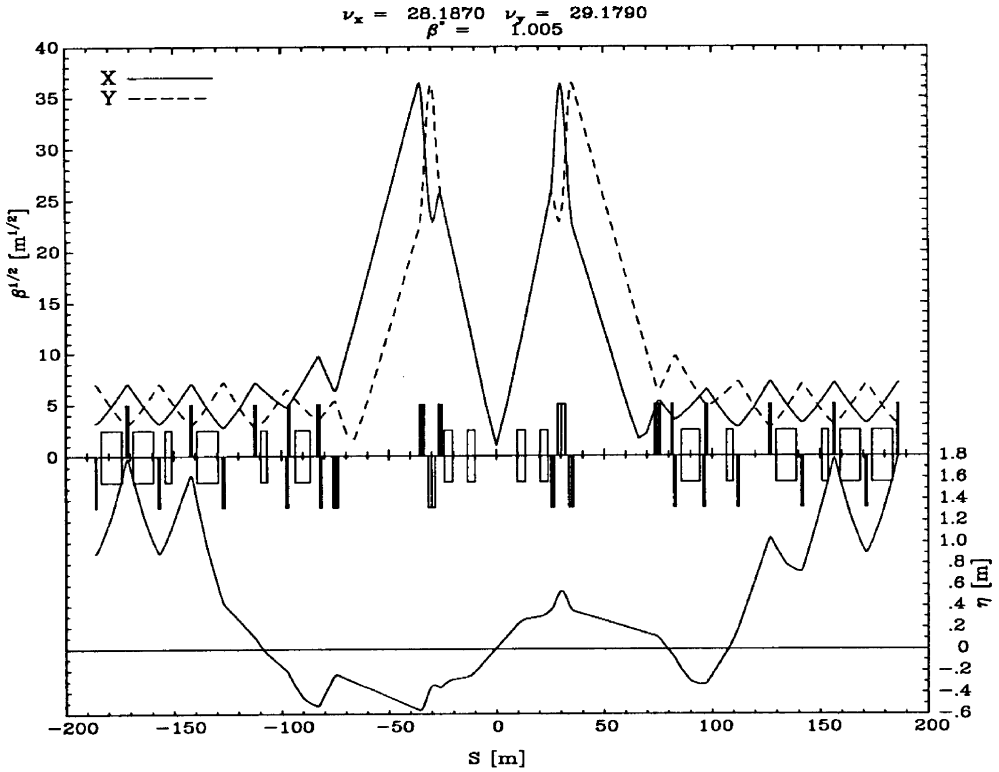

Fig. 6. Insertion functions at $\beta^* = 1$ m.

The optical requirements at the interaction point with regard to amplitude functions, β^*_H, β^*_V, and dispersion, $\eta_H = 0$, $\eta_V = 0$, are satisfied in the insertions. Five half-cells in the insertions, Q10–Q5, with reduced bending due to short dipoles serve as the dispersion suppressor. A residual dispersion due to D0 and DX is taken out by the subsequent quadrupoles. The low-beta function at the interaction point is obtained from an ensemble of five quadrupoles on either side of the IP, divided into two groups: a compact triplet (Q1, Q2, Q3) nearest the crossing point and a doublet (Q4, Q5), separated by a 35 m warm region. These quadrupoles act as a telescope to tune the crossing point to a waist with β^* ranging from 10 m down to about 1 m, for which Fig. 6 displays the lattice functions. The lattice is adjusted to $\beta^* = 10$ m for injection, and during acceleration it is brought to $\beta^* = 6.5$ m which is optimal for transition crossing.

At the end of the acceleration, that is at the beginning of storage and collision, those regions with experiments will be tuned to a low value of β^* to reach the desired luminosity. The beta function in these quadrupoles increases to 667 m at $\beta^* = 2$ m and 1318 at $\beta^* = 1$ m from the 146 m at $\beta^* = 10$ m which represents the optical match to the arc magnet aperture. Hence the aperture of the triplet quadrupoles and of the D0 magnet was enlarged to 13 and 10 cm, respectively, but in spite of this enlargement, it follows that operation with low-beta configurations is limited to energies above 30 GeV/u and requires local magnetic error correctors. The schematic layout of the triplet cryostat assembly with the DO dipole, the Q1, Q2, Q3, quadrupoles and the triplet correctors is shown in Fig. 7. In order to achieve the highest luminosity field quality in these elements sophisticated compensation techniques were developed, including error correction with tuning shims,

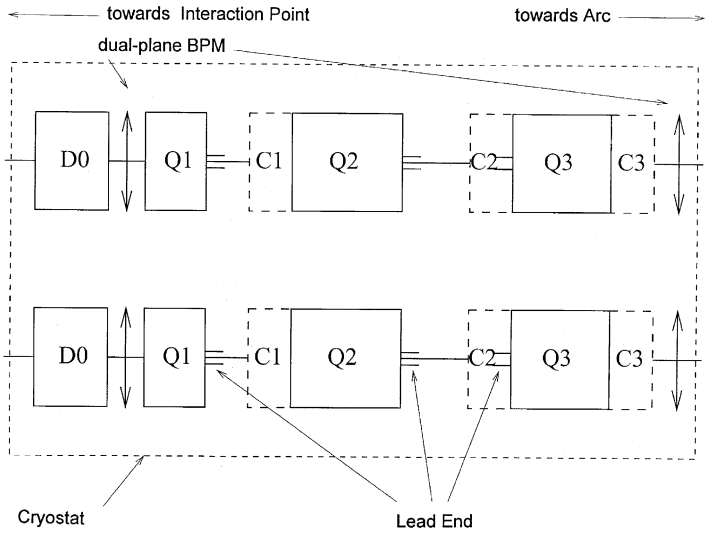

Fig. 7. Schematic layout of the RHIC triplet cryostat assembly.

amplitude-dependent body-ends compensation, low-beta sorting, and the lumped triplet multilayer corrector packages [11].

In the dispersion-matching section between the end of the arc at Q10 and Q4, there are a number of quadrupoles (Q6, Q7, Q8, Q9) equally spaced at the same distance from each other as in the arcs. They represent the natural extension of the arc by adding two regular FODO cells. Special length dipoles are located here with the goal of controlling dispersion at the interaction points and providing dispersion matching, whereas the quadrupoles are set independently for the overall matching of the amplitude functions. It is in this region that injection takes place in the 6 o'clock locations, with the magnetic septum between Q7 and Q8 and the injection kicker in a short warm section between Q9 and a shortened dipole D9. Magnets are located symmetrically around the crossing point and the analogous quadrupoles at the two sides are set at exactly the same excitation but with opposite sign. The nine insertion quadrupoles provide the variable matching section between the final focus and the arc section. The large gradient changes in Q4, Q5 and Q6 are obtained with adjacent trim quadrupoles. During the β^*-squeeze the phase advance across the insertion need not be kept constant, and the change can be absorbed in the regular FODO cells in the arcs. Betatron tunes are adjusted with the regular arc quadrupoles QF and QD over a range of ± 1 unit.

Table 1 gives the summary of the most important global parameters for RHIC. The betatron tunes are split by one unit at $\nu_H = 28.19$ and $\nu_V = 29.18$. The integral part is chosen halfway between 27 and 30 which are multiples of the ring superperiodicity. The fractional part is chosen close to the diagonal in a triangular region between systematic sixth and fifth order resonances, yielding an extension of about 0.033 free of 10th and lower order resonances. The tunes are relatively higher than at other hadron colliders, due to the relatively strong focusing properties. As a result, the transition energy $\gamma_T = 22.89$ is also high and since all ion species are injected into RHIC with $\gamma = 10.5$, transition crossing occurs for all ions except protons which are injected at $\gamma = 25.94$.

4.3. Transition crossing

With the exception of protons, all ions are injected below the transition energy and, consequently, have to be accelerated through transition to reach the top energy for storage. The

acceleration is provided by the 28.15 MHz RF system. In order to successfully transfer the ion beams from the acceleration RF system to the storage RF system at 197 MHz, it is of primary importance to avoid particle loss and to preserve the initial bunch area during the transition crossing.

Since the acceleration rate in a superconducting magnet ring is low, $d\gamma/dt = 1.6\,s^{-1}$ in RHIC, crossing transition energy at slow speed can cause a number of effects. Problems related to transition crossing are mainly divided into two categories: single- and multi-particle. The former category includes the effect of chromatic non-linearities which impel particles of different momenta to cross transition at different times, while the latter includes bunch-shape mismatch and microwave instability induced by low- and high-frequency self-fields, respectively. In fact, the longitudinal coupling impedance limit is largely determined by the transition conditions, where incidentally the compensation of the capacitive space charge by inductive components remains an open question. In addition, the residual voltage of the 197 MHz RF cavities induced by the circulating beam can cause further complication.

Both analytical and numerical studies have been performed to investigate the various problems [17]. It has been shown that the transition crossing can be achieved with no particle loss and negligible bunch-area growth, when a γ_T jump of 0.8 unit is employed in a time period of 60 ms. The chromatic non-linearities are minimized by choosing a lattice with $\beta^* \approx 5$ m, which makes the momentum dependence of the momentum compaction factor, the so-called $\alpha_{1,}$ to zero. A symmetric jump of 0.8 units can be achieved by using a first-order matched γ_T jump involving two quadrupole families and this solution is used in the RHIC lattice [18].

There are two gamma-T families per ring, with four associated quadrupoles in each sextant. The quadrupoles are built into the corrector magnets attached to the 8 cm quadrupoles. In each sextant, the "gt"-group of four is located in the arcs at focusing quadrupoles where the horizontal beta function and dispersion are maximum. In the ideal configuration of 90° per cell, the quadrupole pairs build two π-dispersion bumps, without changing the beta functions outside this group. Thus, this family provides a strong effect on the transition energy, essentially linearly dependent on the quad excitation, but it simultaneously increases the horizontal tune. A second group of four "qt"-quadrupoles is added in the two half-insertions of the sextant, where the dispersion is almost zero and can be used to correct for any tune change. These latter families are arranged in pairs of quadrupoles (denoted as doublets) with phase differences of close to $\pi/2$ to cancel any betatron waves. However, the phase shift per cell of 75° in the RHIC lattice is not ideal and excitation of the gt quadrupoles leads to a small increase in betatron aperture requirement and an increased dispersion from 1.8 to 2.3 m. For the nominal bunch area of <0.5 eV s/u, the physical aperture requirements remain below the good field aperture of ± 27 mm in the arcs.

There are two γ_T power supplies per sextant of each ring. The gt-power supplies must supply ± 28 A for a $\Delta\gamma = \pm 0.4$ jump. The concomitant tune change of ~ 0.28 is corrected by the qt-power supplies by providing an opposite current of comparable strength. The required change of the γ_T is thus obtained with one half of the "nominal" $I = 50$ A power supply capability.

4.4. Chromaticity correction

Compared to other accelerators, the RHIC lattice exhibits relatively strong chromatic effects as a result of the strong focusing arc cells and the long insertions. If the insertions are all identical and set up for $\beta^* = 10$ m the natural chromaticities ($\chi = dvp/dp$) are $\chi_H \sim \chi_V \sim -42$ to which the six arcs contribute -23 units. Lowering β^* to 2 m increases the chromaticity by 12 per insertion. These large negative values of the chromaticities must be reduced to zero or a small positive value.

The chromaticity can be corrected by two families of sextupoles located at quadrupoles where there is significant dispersion. A simple configuration with 12 SF sextupoles next to focussing quadrupoles and SD sextupoles next to defocusing quadrupoles in the arcs provides a first-order correction. The beta and dispersion lattice functions show a residual dependence on

momentum. Independently powered sextupole magnets are provided in the insertion triplets at Q3 to allow local lattice function correction. Furthermore, all the leads to the sextupoles are available so that the number of sextupole families could be increased for better compensation.

4.5. Higher order corrector magnets

The basic lattice configuration with dipoles, quadrupoles and sextupoles would be completely adequate to assure stable motion of single particles assuming ideal properties of all magnet elements. Furthermore, an accurate alignment of the triplet assembly is crucial for the low-beta heavy-ion operation. An accurate alignment of the arc C–Q–S assembly is important for the polarized proton operation. A magnet antenna technique is used to locate the centers of the triplet magnets with an accuracy of better than 0.1 mm. But in spite of the best efforts, real magnets depart unavoidably from the ideal situation and will exhibit systematic errors due to design or intrinsic material properties such as iron saturation or superconductor magnetization and random errors due to fabrication and remaining installation tolerances. Proper operation of the collider as built therefore requires additional systematic trim and random error correction magnets.

The primary objectives for the correction of beam optics distortions are to assure that the orbit is centered in the good field aperture of the magnets, that the fractional tune remains in a range from 0.166 to 0.20, which is free from 10th order and lower resonances (or in the range from 0.2 to 0.25 which is free from 7th and lower resonances). The nominal tune selected for RHIC at $\nu_H = 28.18$ and $\nu_V = 29.19$ is located between the 5th order systematic resonance and the 6th order resonance yielding a useable tune range of 33×10^{-3}.

First in the line of additional corrector magnet systems for RHIC are skew quadrupoles to allow decoupling of horizontal and vertical betatron motion. Skew quadrupoles are located at the 8 cm insertion quadrupoles and extend into two arc quadrupoles for global decoupling. One more skew quadrupole in each triplet Q2 allows local coupling correction.

Achieving a low β^* of 2 m, or even 1 m at the interaction point results in large beta-max values, in the triplet quadrupoles, so that "6σ" beam sizes exceed the nominal "2/3" good field aperture of the triplet magnets. In order to allow operation in these extreme situations, higher order correctors are provided locally in the triplets. Three four-layer corrector packages provide sextupole, octupole, decapole, dodecapole, skew-sextupole, skew-octupole, and skew-decapole magnets.

5. Collider luminosity and performance limitations

The RHIC design is based on utilizing bunched beams colliding head-on to enhance the luminosity while keeping the average current and stored beam energy low. In the asymmetric lattice adopted and assuming full coupling, the bunches are round at the interaction point and the storage RF system keeps the rms bunch length much shorter than the β^*. The luminosity L per interaction point is then given by

$$L = \frac{3}{2} f_{\mathrm{rev}} \frac{\beta\gamma}{\varepsilon_N} \frac{B N_B^2}{\beta^*}$$

where f_{rev} is the revolution frequency, β and γ are the usual kinematic variables, ε_N the normalized transverse emittance, β^* the betatron amplitude function at the interaction point, B the number of bunches, and N_B the number of particles per bunch. The initial number of particles per bunch and the transverse emittance is in the case of heavy ions limited by the available ion source and the injector chain. The beta function at the interaction point is determined by the lattice insertion design and represents the primary method of optimizing luminosity. The bunch length, σ_l, determines the interaction diamond, $\sigma_I = \sigma_l\sqrt{2}$, but since $\sigma_l \ll \beta^*$ it has little influence on the luminosity. The *initial* luminosity for Au–Au collisions at 100 GeV/u and design parameters is $1 \times 10^{27}\,\mathrm{cm}^{-2}\,\mathrm{s}^{-1}$. At lower energies, the initial luminosity will decrease linearly with energy.

In contrast to typical hadron colliders, the beam–beam tune shift is small for the design gold

intensities and does not limit the performance. The beam–beam parameter, i.e. the tune shift per interaction region, is independent of energy and β^* and given by

$$\xi = \frac{3r_p}{2}\frac{Z^2}{A}\frac{N_B}{\varepsilon_N}$$

with r_p the classical proton radius and Z and A the atomic and mass number. At the design values, one finds for Au–Au collisions a tune shift of $\xi = 0.002$ for one 2 m insertion, well below the quoted limit of 0.004.

The luminosity decreases during the storage time from the initial value due to loss of particles and emittance blow up, phenomena which depend on the ion species and several machine factors. If the average luminosity has fallen below a useful value, the beam is aborted and a new cycle is initiated. The beam–beam or interbeam nuclear reaction is the purpose of constructing the collider; yet this process also contributes to beam loss. For ions with $A<100$ the desired nuclear reactions dominate the lifetime of the beam. For heavier ions, especially for the prototypical case of gold, the luminosity lifetime is predominantly determined by intrabeam scattering [19], which results in emittance blow up but also particle loss from bunch area growth beyond the bucket area.

Intrabeam scattering is caused by particles in the same bunch exchanging longitudinal and transverse momenta by Coulomb scattering, which depends on the charge Ze and on the mass number A of the ions. The scattering cross-section is proportional to $(Z^2/A^2)^2$, which for high Z leads to severe limitations from intrabeam scattering. Reliable predictions for the emittance and bunch area growth due to intrabeam scattering have been obtained by numerical integration of the relevant set of differential equations taking into account the variation of the betatron and dispersion functions around the ring. Qualitative results which are adequate to estimate performance can be obtained, assuming full coupling, from the following approximations for the transverse and longitudinal diffusion times τ_H and τ_E, respectively, which are valid above transition and in first order independent of the beam energy [4,19,20]

$$\tau_H^{-1} = \frac{1}{\sigma_H}\frac{d\sigma_H}{dt} = \frac{27\pi}{4} L_C r_p^2 E_0 \frac{\langle\eta_H\rangle}{\langle\beta\rangle}\left\{1+\left(\frac{\langle\sigma_H\rangle}{\eta_H\delta_E}\right)^2\right\}^{-1/2} \times \frac{N_B}{S\varepsilon_H\varepsilon_V}\left(\frac{Z^2}{A}\right)^2$$

and

$$\tau_E^{-1} = \frac{1}{\delta_E}\frac{d\delta_E}{dt} = 2\left\{\frac{\langle\sigma_H\rangle}{\eta_H\delta_E}\right\}^2 \tau_H^{-1}$$

where $L_C \approx 20$ is the Coulomb logarithm, r_p the classical proton radius, S the bunch area per nucleon, ε_N the normalized transverse emittances, $\langle\beta\rangle$, and $\langle\eta_H\rangle$, the betatron function and dispersion averages and $\langle\sigma_H\rangle$ the transverse rms beam size. In the early phase of the storage cycle, the energy spread increases rapidly until an equilibrium at $\langle\eta\rangle\delta_E \approx \sqrt{2}\sigma_H$ is reached. Later on, particle loss starts when the beam dimensions reach the magnet aperture or the RF bucket limit. Estimates for gold indicate that the transverse emittance grows from 10 to about 40 π mm mrad and that the bucket area of 1.2 eV s provided by the 6 MV storage RF system is too limited and particle loss of as much as 40% in 10 h occurs. Fig. 8 shows the luminosity reduction caused by IBS emittance growth and beam loss during a store [11]. The luminosity lifetime of gold beams is expected to be about 10 h resulting in an average luminosity of $2\times10^{26}\,\mathrm{cm}^{-2}\,\mathrm{s}^{-1}$.

Nuclear scattering between the ion beam and residual gas leads to beam loss and background radiation near the experimental detectors and establishes the vacuum specifications in the warm sections [21]. In the absence of vacuum leaks, the cold bore sections at 4 K have excellent vacuum, with a He density equivalent to $\sim10^{-12}$ mbar. The warm sections, which present ~17% of the ring circumference, require a vacuum pressure of better than 5×10^{-10} mbar. In a vacuum of this quality, transverse beam growth due to multiple small angle scattering on the residual gas molecules is insignificant.

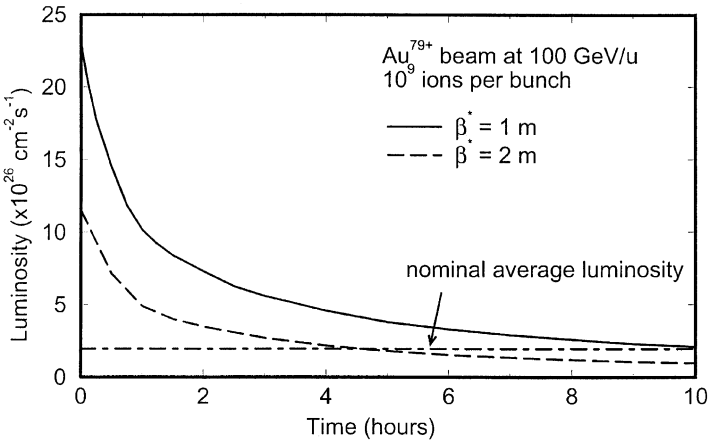

Fig. 8. Luminosity reduction caused by intrabeam scattering.

For ions with mass number $A > 100$, additional beam depleting phenomena that are unique to heavy-ion colliders play a non-negligible role. To be mentioned are two Coulomb-induced processes occurring during beam crossing that provide limits on the beam lifetime, dissociation of the nucleus and production of electron–positron pairs that result in spontaneous capture of the electron in a bound orbital of an ion [22]. Coulomb dissociation will most often result in the emission of 1–3 neutrons and the fragments fall out of the beam. In the pair production, an electron is produced in a bound state of the ion, thereby changing the charge of the ion. These mass or charge-changing reactions cause the ion to be lost from the beam and thus reduce the luminosity.

Unlike intrabeam scattering, which is sensitive to the ion charge and mass, Coulomb dissociation and spontaneous electron capture depends only on the charge of the ion. For collision of equal ion species, Coulomb dissociation scales as $Z^{8/3}$ and spontaneous electron capture scales as Z^7. Further it is noted that as the beam energy increases intrabeam scattering becomes relatively less important, but both Coulomb dissociation and capture cross-sections grow with beam energy. The particle intensity loss rate is given by

$$\frac{\mathrm{d}N_\mathrm{B}}{N_\mathrm{B}\mathrm{d}t} = -\frac{N_\mathrm{C}}{BN_\mathrm{B}} L\sigma_\mathrm{T}$$

where N_C is the number of collision regions and $\sigma_\mathrm{T} \approx 250 \times 10^{-24}\,\mathrm{cm}^2$ is the accumulative cross-section for the so-called nuclear depleting reactions, including Coulomb dissociation, spontaneous electron capture, and central nuclear collisions. Initial luminosity half-life due to these effects is ~ 8 h, assuming four low beta insertions with $\beta^* = 2$ m. In order to estimate the actual time dependence of the collider luminosity, it would be necessary to solve the above equation self-consistently including particle losses and emittance growth due to intrabeam scattering. The beam loss due to nuclear reactions beyond intrabeam scattering could reduce the average luminosity in RHIC by an additional $\sim 25\%$.

Overall, the luminosity lifetime of a heavy-ion collider will be sensitive to a number of beam and machine parameters. Complete knowledge of some of these parameters, not the least those causing coupling impedance induced collective effects, will not be available until sufficient operational experience at design level is available.

References

[1] T. Ludlam, A. Schwarzschild, Nucl. Phys. A 418 (1984) 657c.
[2] M.Q. Barton, H. Hahn, Nucl. Phys. A 418 (1984) 329c.
[3] H. Hahn, Part. Accelerators 32 (1990) 1517.

[4] H. Foelsche, H. Hahn, M. Harrison, S. Ozaki, M.J. Rhodes-Brown, in: H. Schopper (Ed.), Advances of Accelerator Physics and Technologies, World Scientific, Singapore, 1993, p. 104.
[5] P. Thieberger, Nucl. Instr. and Meth. 220 (1984) 45, 209.
[6] P. Thieberger, M. McKeown, H.E. Wegner, IEEE Trans. Nucl. Sci. NS-30 (4) (1983) 2746.
[7] A.G. Ruggiero, Nucl. Instr. and Meth. A 328 (1993) 3; A.G. Ruggiero, Report BNL-35127, 1984.
[8] J. Kewisch, V. Ptitsin, J. Rose, J. Wei, Report RHIC/AP/145, 1997.
[9] H. Hahn, A. Dunbar, C.I. Pai, R.T. Sanders, N. Tsoupas, Proceedings of the 1999 PAC, Vol. 2, New York, 1999, p. 1100.
[10] P.A. Thompson, et al., Proceedings of the 1991 Particle Acc. Conference, San Francisco, CA, p. 2245.
[11] J. Wei, M. Harrison, in: K. Hatanaka, et al. (Eds.), Proceedings of the XVI RCNP Osaka International Symposium on Multi-GeV High-Performance Accelerators, Osaka, Japan, World Scientific, Singapore, 1997; J. Wei, M. Harrison, BNL Report RHIC/AP/123, 1997.
[12] R.C. Gupta, et al., Proceedings of the 1999 Part. Acc. Conference, New York, NY, p. 185.
[13] J.H. Sondericker, in: R.J. Donnelly, K.R. Sreenivasan (Eds.), Flow at Ultra-High Reynolds and Rayleigh Numbers, Springer, New York, 1998, p. 315.
[14] D.P. Brown, R.J. Gibbs, A.P. Schlafke, J.H. Sondericker, K.C. Wu, in: R.W. Fast (Ed.), Advances in Cryogenic Engineering, Vol. 33, Plenum Press, NY, 1987, p. 663.
[15] S.Y. Lee, J. Claus, E.D. Courant, H. Hahn, G. Parzen, Proceedings of the 1985 Part. Acc. Conf., Vancouver, BC, p. 1626.
[16] S. Tepikian, V. Mane, S. Peggs, BNL Report AD/RHIC/AP-23, 1994.
[17] J. Wei, Proceedings of the EPAC 92, Vol. 1, Berlin, p. 643.
[18] S. Peggs, S. Tepikian, D. Trbojevic, Proceedings of the 1993 Part.Acc. Conference, Vol. 1, Washington, DC, p. 169.
[19] G. Parzen, Nucl. Instr. and Meth. A 251 (1986) 220; G. Parzen, Nucl. Instr. and Meth. A 256 (1987) 231.
[20] J. Wei, Proceedings of the 1993 PAC, Vol. 5, Washington, DC, p. 3651.
[21] M.J. Rhoades-Brown, M. Harrison, BNL Report AD/RHIC-106, 1991.
[22] A.J. Baltz, M.J. Rhodes-Brown, J. Weneser, Phys. Rev. E 54 (1996) 4233.